Enhanced Empirical Wavelet Transform for Denoising of Fundus Images

C. Amala Nair and R. Lavanya(✉)

Department of Electronics and Communication Engineering,
Amrita School of Engineering, Coimbatore,
Amrita Vishwa Vidyapeetham, Coimbatore, India
amalanairc@gmail.com, r_lavanya@cb.amrita.edu

Abstract. Glaucoma is an ophthalmic pathology caused by increased fluid pressure in the eye, which leads to vision impairment. The evaluation of the Optic Nerve Head (ONH) using fundus photographs is a common and cost effective means of diagnosing glaucoma. In addition to the existing clinical methods, automated method of diagnosis can be used to achieve better results. Recently, Empirical Wavelet Transform (EWT) has gained importance in image analysis. In this work, the effectiveness of EWT and its extension called Enhanced Empirical Wavelet Transform (EEWT) in denoising fundus images was analyzed. Around 30 images from High Resolution Fundus (HRF) image database were used for validation. It was observed that EEWT demonstrates good denoising performance when compared to EWT for different noise levels. The mean Peak Signal to Noise Ratio (PSNR) improvement achieved by EEWT was as high as 67% when compared to EWT.

Keywords: Denoising · Glaucoma · Empirical Wavelet Transform
Enhanced Empirical Wavelet Transform · Peak Signal to Noise Ratio

1 Introduction

Glaucoma is the second common source of vision loss usually seen in the age group of 40–80 years. It is characterised by very high eye pressure, which damages the Optic Nerve Head (ONH) causing peripheral vision loss and finally leading to blindness [1]. Approximately 64.3 million people in the world were suffering from glaucoma in 2013. By 2020 this number might rise to 76 million and by 2040 it might affect 111.8 million people [2]. Although glaucoma cannot be cured, timely treatment will help to hold back its progression. Therefore, diagnosis of this disease is important to avoid preventable vision loss [3].

The diagnosis necessitates regular eye tests, which is expensive and time - consuming. Conventional diagnosis techniques are based on manual observations and hence restricted by the expertise of ophthalmologists in the domain and prone to inter observer variability [1]. These limitations impose the need for automated methods which offer consistency, objective analysis and time efficiency. Among the various imaging modalities used for glaucoma detection, digital fundus photography is preferred for automated diagnosis since it is cost effective and captures a large retinal field.

I. Zelinka et al. (Eds.): ICSCS 2018, CCIS 837, pp. 116–124, 2018.
https://doi.org/10.1007/978-981-13-1936-5_13

Clinical information suggests that the ONH examination is the most beneficial method for diagnosing glaucoma structurally. Proper segmentation of structures in and around ONH requires precise identification of the border between the retina and the rim which has a number of limitations [4]. The accuracy of the system developed relies on the accuracy of segmentation performed.

Among the various techniques used for image analysis, wavelet transform has shown to have an upper hand. The drawback of wavelet analysis is that it has fixed basis and hence is non-adaptive with respect to signal characteristics [5]. Huang et al. [6] propounded Empirical Mode Decomposition (EMD) which is adaptive in nature. It decomposes the non- stationary signal into modes known as Intrinsic Mode Functions which acts as the bases. EMD makes use of a process known as sifting for signal decomposition. However, there are a few shortcomings of EMD, such as lack of a strong theoretical background, no robust stopping criterion for sifting process, mode mixing and end effects [7].

To overcome the limitations of EMD, Empirical Wavelet Transform (EWT) was suggested [8] and it is shown to have an upper hand over other time-frequency analysis methods [9, 10]. By combining the time-frequency localisation properties of wavelets and adaptability of Empirical Mode Decomposition (EMD), EWT is found to be apt for analysing fundus images. However, EWT does not take spectrum shape into consideration while performing segmentation of the spectrum to decompose images into different modes. The drawback of EWT was identified and a new approach was proposed by Hu et al. [11] known as Enhanced Empirical Wavelet Transform (EEWT). It makes use of an envelope-based approach using the Order Statistics Filter (OSF) for segmentation of the Fourier spectrum. EEWT is found to have better performance for non-stationary signal analysis [10].

Fundus images are generally affected by additive, multiplicative noise and a mixture of these two [12]. EWT has shown to have an upper hand in Computer Aided Detection (CAD) systems for diagnosing glaucoma. In such systems, as a preprocessing step, techniques like Median and Gaussian filters are used for denoising the fundus images [13]. Rather than making use of an additional preprocessing step, the inherent denoising ability of EWT and EEWT can be utilized. The purpose of the work is to study the effects of EWT and EEWT in denoising of fudus images.

This paper is arranged as follows. Section 2 gives a summary of the two techniques used and the methodology adopted. Section 3 covers the results and discussions. Finally, the paper concludes in Sect. 4.

2 Methodology

This work focuses on analyzing EWT and its extension EEWT on fundus images. EWT and EEWT were applied on the fundus images to form sub images from low to high frequency. Next, the modes were thresholded to eliminate the effect of noise. Inverse transform was performed on these modes to reconstruct the signal. EWT, EEWT and the denosing method employed are explained in Sects. 2.1, 2.2 and 2.3.

2.1 Empirical Wavelet Transform

Gilles [8] proposed EWT in order to analyse signals such that adaptability of EMD and time frequency localisation of wavelets can be combined together. EWT decomposes the signal into modes using wavelet filter banks, whose supports are derived from the location of information in the signal. The main steps involved in EWT are segmentation of the spectrum followed by construction of EWT basis and their application on the segments formed. For N segments, a bank of filters will be defined; N−1 band pass filters and a low pass filter. The procedure involved in EWT is illustrated in Fig. 1.

Segmentation of the signal spectrum requires dividing it into N continuous segments given as $\lambda_n = [\omega_{n-1}\omega_n]$, where ω_n is the frequency at any point n. Centered on each ω_n, a transition phase T_n is defined with a width of $2\tau_n$. Excluding 0 and π, N−1 boundaries should be detected. They are obtained by finding all the local maxima of the spectrum and sorting them in descending order. The first N−1 maxima are then selected. Boundaries are found as the average between the positions of two consecutive maxima. Empirical scaling and wavelet functions are obtained similar to Littlewood-Paley wavelets and Meyers wavelets. For the signal spectrum $v(\omega)$, empirical scaling function and empirical wavelet function are shown as Eqs. (1) and (2) respectively.

The empirical scaling function is defined as:

$$\phi_n(\omega) = \begin{cases} 1 & \text{if } |\omega| \le \omega_n - \tau_n \\ cos\left[\frac{\pi}{2} v\left(\frac{1}{2\tau_n}(|\omega| - \omega_n + \tau_n)\right)\right] & \text{if } \omega_n - \tau_n \le |\omega| \le \omega_n \\ 0 & \text{otherwise} \end{cases} \tag{1}$$

The empirical wavelet function is defined as:

$$\psi_n(\omega) = \begin{cases} 1 & \text{if } \omega_{n-1} - \tau_{n-1} \le |\omega| \le \omega_{n-1} - \tau_{n-1} \\ cos\left[\frac{\pi}{2} v\left(\frac{1}{2\tau_{n+1}}(|\omega| - \omega_{n+1} + \tau_{n+1})\right)\right] & \text{if } \omega_{n+1} - \tau_{n+1} \le |\omega| \le \omega_{n+1} + \tau_{n+1} \\ sin\left[\frac{\pi}{2} v\left(\frac{1}{2\tau_n}(|\omega| - \omega_n + \tau_n)\right)\right] & \text{if } \omega_n - \tau_n \le |\omega| \le \omega_n + \tau_n \\ 0 & \text{otherwise} \end{cases} \tag{2}$$

By taking the inner product between signal and empirical wavelet function, wavelet coefficients can be obtained. Similarly, the inner product of signal with empirical scaling function gives the scaling coefficient.

This concept was extended to images in [14] by Gilles et al. The empirical counterpart of Tensor wavelets, Curvelets, Littlewood-Paley wavelets and Symlets were built. In 2 dimensional Littlewood-Paley wavelet transform, images are filtered using wavelets with annuli supports. Hence, Polar FFT is preferred in this case. Pseudo polar FFT is a method which helps to do this with less computational complexity since FFT is computed on a square grid rather than polar grid [15].

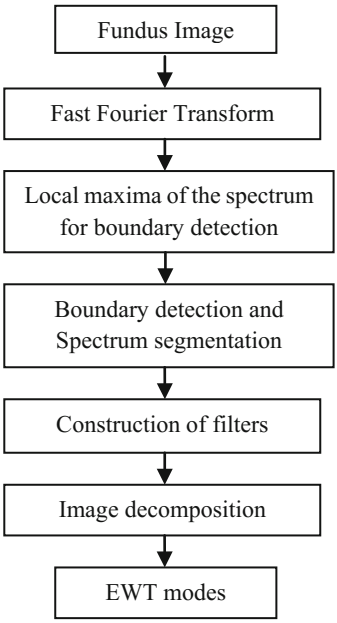

Fig. 1. Flowchart of EWT

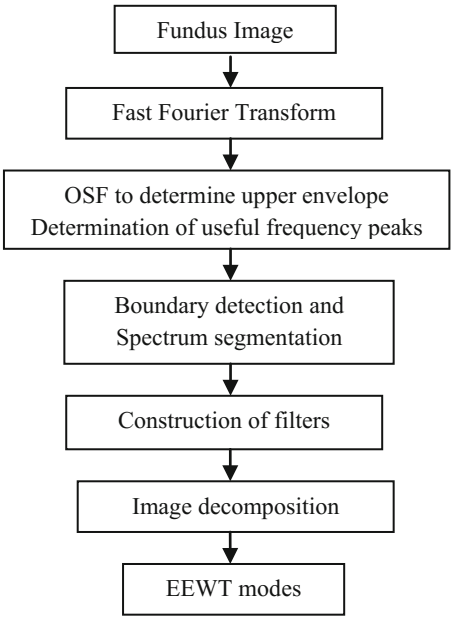

Fig. 2. Flowchart of EEWT

2.2 Enhanced Empirical Wavelet Transform

EWT is limited by the fact that it can be used to analyze signals with well separated frequencies. For signals that are noisy, or non-stationary in nature, EWT may not perform well, as the boundary detection may result in errors. The local maxima, which might be significant may not be considered while those which are part of the noise might be considered. Segmentation performed with such boundaries will be incorrect. This drawback is a result of spectrum shape not being considered by EWT. On the other hand, EEWT considers the spectrum shape for segmentation of the signal.

In EEWT, OSF is first applied on the input signal to obtain the upper envelope from which the major peaks are found. The procedure involved in EEWT analysis is illustrated in Fig. 2.

FFT of the signal is taken in order to obtain the spectrum. OSF is performed on the spectrum using Max filter for upper envelope detection. A sliding window of size s_{OSF} centered at a point is used to determine the upper envelope (U) at that point as the maximum value of elements in that region. The upper envelope is given by (3)

$$U(n) = \max_{k \epsilon A_n}(D(k)) \tag{3}$$

where D denotes the sequence of data and A_n denotes the sliding window. At any point n, the value of U is the maximum value of D over the region A_n. The size of sliding window is found by considering all the local maxima. The minimum value of the

Euclidean distance between two consecutive local maxima gives the value of s_{OSF} given by (4)

$$s_{OSF} = \min\{D_{max}\} \tag{4}$$

where D_{max} is an array containing the Euclidean distance between consecutive local maxima of the data.

When OSF is applied on a signal, any peak in the signal spectrum becomes a flat top. These useful flat tops corresponding to the most significant peaks will be used for boundary detection. For this purpose, the following three criteria are used.

Criterion 1: Significant flat tops have width greater than or equal to the size of OSF.

Criterion 2: Within a neighbourhood the flat top with maximum value is the significant one. Neighborhood for a flat top is its preceding flat top and the flat top before the previous one.

Criterion 3: The flat tops obtained from the downward trend of the signal spectrum are not considered as useful ones.

Boundary detection involves choosing the lowest among consecutive flat tops. Once the boundary is detected, the spectrum is segmented in accordance with the boundary obtained. Following this, filter banks are constructed and the signal is decomposed using the filters.

2.3 Denoising Using EWT/EEWT

Soft thresholding is applied on EWT modes to remove noise. The threshold value was found using Eq. (5).

$$\tau = \sigma\sqrt{2\log(M)} \tag{5}$$

where τ is the universal thresholding, M represents the total number of pixels in the image and σ gives the noise level estimate. It is given by Eq. (6).

$$\sigma = \frac{median\{w\}}{0.6745} \tag{6}$$

where w is the wavelet coefficient.

EEWT can distinguish noise and meaningful components effectively boundaries detected are optimal. Thus denoising was performed by removing the mode containing the highest frequency.

3 Results and Discussions

A total of 30 retinal fundus images were acquired from High Resolution Fundus (HRF) image database [16]. MATLAB R2017a on Windows platform was used for the implementation of this work. For validation of the denoising performance, Speckle and

Gaussian noise were added to the images, followed by decomposition of the images into EWT and EEWT modes. Figure 3 shows the green channel of fundus image decomposed into modes using EWT. Figure 4 shows the decomposition of images using EEWT.

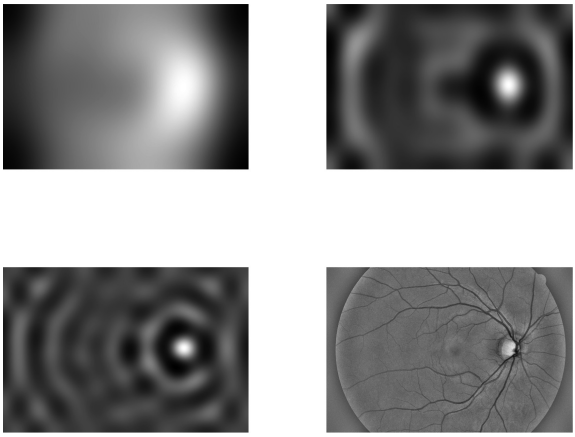

Fig. 3. Decomposition using EWT

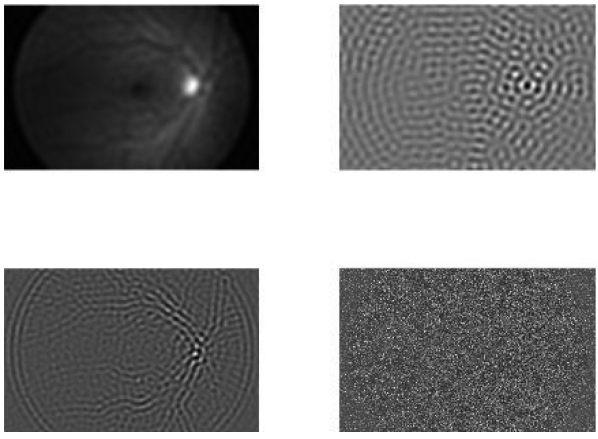

Fig. 4. Decomposition using EEWT

Denoising was performed using EWT and EEWT methods. By comparing the sub-band images of EWT and EEWT, it is clear that noise is more distinguishable in EEWT than EWT. Further, in EEWT, the low frequency content was retained without much noise in the first intrinsic mode function. High frequency components clearly show the

influence of noise. On the other hand, in EWT, it is difficult to distinguish between noise and meaningful content since noise gets mixed in all modes. This shows that spectral boundaries detected for EEWT are optimal as compared to EWT.

These cases were considered with different values for noise variance. Images were corrupted by Speckle and Gaussian noise with variance of 0.001, 0.01 and 0.05 respectively. Figure 5 shows images corrupted by noise with variance of 0.05, EWT and EEWT denoised images.

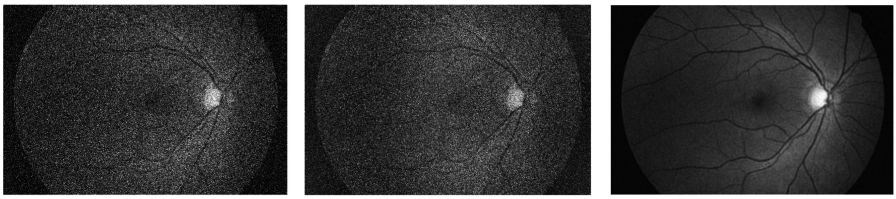

(a) (b) (c)

Fig. 5. (a) Image with noise variance 0.05, (b) Denoised using EWT, (c) Denoised using EEWT

Denoised images of EEWT shows reduced noise levels and thus improved quality when compared to EWT. This indicates that the boundaries detected using EWT could not effectively separate noise from image content. To quantitatively analyze the denoising performances of the two methods, Peak Signal to Noise Ratio (PSNR) was calculated.

Table 1. Mean PSNR values of EWT and EEWT denoising for different noise variance

Noise variance	EWT	EEWT
0.001	26.351 dB	39.256 dB
0.01	19.552 dB	34.209 dB
0.05	14.057 dB	26.723 dB

Table 1 shows the mean PSNR values for EWT based denoising and EEWT based denoising on 30 images for different levels of noise variance. It is seen that the mean performance of EEWT is better than EWT. This can be attributed to the fact that EEWT takes spectrum shape into consideration for segmentation of the spectrum. As a result, EEWT can separate out the insignificant peaks caused by noisy components better when compared to EWT.

It is further observed that EWT is inefficient especially when greater amount of noise is present in the image. On the other hand, EEWT shows good performance even when noise levels are high. Hence EEWT is suitable in analysing glaucoma using fundus images which are susceptible to noise during acquisition process. The inherent denoising capability of the technique alleviates the need for denoising as a pre-processing step.

4 Conclusion

Though much work has been based recently on EWT for image analysis, it can be seen that EEWT is a better alternative for non-structural approach. EEWT has better inherent noise removing capability resulting in an overall improved performance compared to EWT. Thus EEWT, with its combined noise robustness, adaptability and time-frequency localisation is a promising technique for computer aided glaucoma diagnosis.

References

1. Haleem, M.S., Han, L., Hemert, J.V., Li, B.: Automatic extraction of retinal features from colour retinal images for glaucoma diagnosis: a review. Comput. Med. Imaging Graph. **37**, 581–596 (2013)
2. Tham, Y.C., Li, X., Wong, T.Y., Quigley, H.A., Aung, T., Cheng, C.Y.: Global prevalence of glaucoma and projections of glaucoma burden through 2040: a systematic review and meta analysis. Ophthalmology **121**, 2081–2090 (2014)
3. Zhang, Z., et al.: A Survey on computer aided diagnosis for ocular diseases. BMC Med. Inform. Decis. Mak. **14**, 80 (2014)
4. Almazroa, A., Burman, R., Raahemifar, K., Lakshminarayanan, V.: Optic disc and optic cup segmentation methodologies for glaucoma image detection: a survey. J. Ophthalmol. **2015**, 581–596 (2013)
5. Lei, Y., Lin, J., He, Z., Zuo, M.J.: A review on empirical mode decomposition in fault diagnosis of rotating machinery. Mech. Syst. Signal Process. **35**, 108–126 (2013)
6. Huang, N.E., et al.: The empirical mode decomposition and the hilbert spectrum for non-linear and non-stationary time series analysis. Proc. Roy. Soc. Lond. **454**, 903–995 (1998)
7. Xuan, B., Xie, Q., Peng, S.: EMD sifting based on bandwidth. IEEE Signal Process. Lett. **14**, 537–540 (2007)
8. Gilles, J.: Empirical wavelet transform. IEEE Trans. Biomed. Eng. **61**, 3999–4010 (2013)
9. Jambholkar, T., Gurve, D., Sharma, P.B.: Application of empirical wavelet transform (EWT) on images to explore brain tumor. In: 3rd International Conference on Signal Processing, Computing and Control, pp. 200–204. IEEE (2015)
10. Maheshwari, S., Pachori, R.B., Acharaya, U.R.: Automated diagnosis of glaucoma using empirical wavelet transform and correntropy features extracted from fundus images. IEEE J. Biomed. Health Inform. **21**, 803–813 (2017)
11. Hu, Y., Li, F., Li, H., Liu, C.: An enhanced empirical wavelet transform for noisy and non-stationary signal processing. Digit. Signal Process. **60**, 220–229 (2017)
12. Hani, A.F.M., Soomro, T.A., Fayee, I., Kamel, N., Yahya, N.: Identification of noise in the fundus images. In: 3rd IEEE International Conference on Control System, Computing and Engineering, pp. 191–196. IEEE CSS Chapter, Malaysia (2013)
13. Dharani, V., Lavanya, R.: Improved microaneurysm detection in fundus ımages for diagnosis of diabetic retinopathy. In: Thampi, S.M., Krishnan, S., Corchado Rodriguez, J. M., Das, S., Wozniak, M., Al-Jumeily, D. (eds.) SIRS 2017. AISC, vol. 678, pp. 185–198. Springer, Cham (2018). https://doi.org/10.1007/978-3-319-67934-1_17

14. Gilles, J., Tran, G., Osher, S.: 2D empirical transforms. Wavelets, ridgelets and curvelets revisited. SIAM J. Imaging Sci. **7**, 157–186 (2014)
15. Averbuch, A., Coifman, R.R., Donoho, D.L., Elad, M., Israeli, M.: Fast and accurate polar fourier transform. Appl. Comp. Harmon. Anal. **21**, 145–167 (2006)
16. Budai, A., Bock, R., Maier, A., Hornegger, J., Michelson, G.: robust vessel segmentation in fundus images. Int. J. Biomed. Imaging **2013**, 11 (2013)